Fourier Transform Infrared Study of the Rod Outer Segment Disk and Plasma Membranes of Vertebrate Retina†

Om P. Lamba,* Douglas Borchman, and Paul J. O'Brien‡

Department of Ophthalmology and Visual Sciences, University of Louisville School of Medicine, Kentucky Lions Eye Research Institute, University of Louisville, Louisville, Kentucky 40292, and Health Research Associates, 12 Duke Street South, Rockville, Maryland 20850

Received June 25, 1993; Revised Manuscript Received November 24, 1993®

ABSTRACT: Phospholipid composition and structure of disk and plasma membranes purified from bovine rod outer segments (ROS) are examined using Fourier transform infrared spectroscopy. Vibrational data indicate that both disk and plasma membranes lack sphingophospholipids, in contrast to the lens membranes. The hydrocarbon chains of the disk lipids are unsaturated by a *factor of 5* over the acyl chains of the plasma lipids. The plasma lipids with 3-fold higher cholesterol and 5-fold higher saturation melt at a higher temperature (26 °C) than the disk lipids which melt at 16 °C. The transition temperature decreases by more than 20 °C in going from disk lipids to disk membrane, indicating a large drop in the enthalpy of the ROS membrane–matrix, presumably due to enhanced rhodopsin–lipid interaction. The lipid composition predisposes the disk and plasma membranes to be fluid and structurally disordered (about 84%) around physiological temperature. The fluid phospholipid environment of the disk membrane (i.e., just a few degrees above subzero temperatures) is considered to be vital for the ROS photoreceptor function. The amide I band profile of rhodopsin indicates an extensive α-helical (53%) peptide chain, with little β-sheet (21%) and β-turns (18%) in ROS membranes. This structure and/or conformation is conserved between 0–60 °C even though disk and plasma lipids undergo a phase change. The H–D exchange data indicate that as much as 84% of the peptide residues of ROS membranes in partially bleached retinas is accessible to D_2O solvent after 1 h. This (3–4)-fold higher exchange compared to the rate observed in the dark-adapted retinas is understood primarily from the breakdown of hydrophobic interactions and/or tertiary and quaternary structures which stabilize the ROS membranes. It appears that photobleaching not only transduces photons but opens up the "hydrophobic heart" of the rhodopsin which leads to solvent accessibility. The rhodopsin structure may be stabilized through hydrogen bridges existing between phospholipid carbonyls with rhodopsin and/or bilayer water, but hydrophobic forces appear to play a dominant role in stabilizing the ROS membrane–matrix. Subjection of ROS lipids to oxidative stress results in a substantial increase in conjugated polyenes, characteristic of the LPO-induced free-radical damage involving pathological process in retinal disorders. The data indicate structural and chemical modifications of the membrane phosphate headgroup and degradation of the hydrocarbon region similar to those observed in the cataractous lens membranes. A change in lipid order (fluidity) was observed that may derange ROS membrane function. Addition of low amounts of α-tocopherol inhibits lipid oxidation, maintaining the functional integrity of the ROS.

Photoreceptor rod outer segment (ROS) membranes contain the biochemical machinery necessary for the transduction of photons into electrical signals as a part of the visual excitation process. ROS cells are often the first cells in the visual pathway to degenerate or die in dysfunctional retinas from hereditary defects (retinitis pigmentosa), oxidative stress, overexposure to light, toxic agents, and dietary inadequacies such as vitamin A deficiency (Young, 1988). This damage to photoreceptor cells may involve the metabolism of the polyunsaturated fatty-acid-containing lipids and alter their chemical and structural composition which could lead to age-related maculopathy and visual impairment (Yeagle, 1989). Incomplete metabolism or reduced rate of turnover could result in accumulation of lipid peroxidation (LPO) products that may lead to other pathological conditions similar to those associated with retinitis pigmentosa (Zigler & Hess, 1985).

Mammalian ROS cells are rich in polyunsaturated fatty acids (about 50%) characterized by the polyenes of the $n-3$ series, docosahexanoic acid ($22{:}6n-3$) being the most abundant (Fliesler & Anderson, 1983). Such a high content of polyunsaturated hydrocarbon chains especially in the disk membranes (Boesze-Battaglia & Albert, 1989; Lamba et al., 1992) predisposes them as targets for oxidative damage (Anderson & Maude, 1971; Babizhayev & Deyev, 1989). ROS membrane lipid composition is altered upon oxidation (Rotstein et al., 1987; Boesze-Battaglia et al., 1989; Babizhayev & Deyev, 1989), changes in diet (Anderson & Maude, 1971; Speth & Wunderlich, 1973; Carter-Dawsen et al., 1979), light intensity (Kagan et al., 1973; Delmelle & Pontus, 1975; Noell, 1980; Shvedova et al., 1983; Organisciak et al., 1985; Wiegand et al., 1986; Penn & Anderson, 1987), and pathology (Hong & Hubbell, 1972; Bazan & Scott, 1987; Wetzel al., 1990). The oxidized lipids may form pores in the membrane (Noordam et al., 1982) and/or decompose to secondary end products which are capable of cross-linking proteins and other molecules (Leibovitz & Siegel, 1980; Armstrong, 1984). The

† This is paper III in the series Spectral Studies of the Lipids and Proteins of Ocular Tissues. This work was supported by Alcon Laboratories, Inc., Fort Worth, TX, and in part from research grant EY-07975, the Kentucky Lions Eye Foundation, and an unrestricted grant from Research to Prevent Blindness, Inc.

* Author to whom correspondence should be addressed.

‡ Health Research Associates.

® Abstract published in *Advance ACS Abstracts,* February 1, 1994.

0006-2960/94/0433-1704$04.50/0

high content of phosphatidylethanolamine in disk membranes may form headgroup adducts with secondary products of lipid oxidation which may impair rhodopsin regeneration and could derange ROS membrane function.

Besides the unique phospholipid composition, ROS membranes are rich in rhodopsin, 4 and 38 mol of rhodopsin/mol of phospholipid in plasma and disk membranes, respectively (Kamp et al., 1982). Rhodopsin with its seven transmembrane helices, with half the mass virtually buried inside the lipid matrix, is expected to have strong lipid–protein interactions (Ovchinnikov, 1982; Hargrave, 1982). A number of NMR (Brown et al., 1976; DeGrip et al., 1979), ESR (Hong & Hubbell, 1972; Pontus & Delmelle, 1975), and fluorescent probe studies (Stubbs et al., 1976a; Sklar et al., 1979) have indicated that rhodopsin is surrounded by an annulus of 24 lipid molecules whose lateral diffusion is impeded, evidence that rhodopsin–lipid interactions do exist. The functional activity of the rhodopsin thus depends upon the lipid environment, i.e., high hydrocarbon fluidity, low cholesterol content (O'Brien et al., 1977; Morton et al., 1986), headgroup composition, and bilayer thickness (O'Brien et al., 1977).

In this paper, we explore the phospholipid environment (structure and composition) of the bovine ROS membranes using FTIR spectroscopy. To fully understand retinal–opsin interactions, detailed information about the molecular structure and conformation of rhodopsin in the lipid matrix is required. Molecular spectroscopy, infrared or Raman, is uniquely suited to probe such features in the ROS membranes. Oxidative damage to ROS membranes is also assessed. Free-radical damage associated with retinal degeneration is the principal underlying cause of visual impairment. The present work provides evidence of complete inhibition of the free-radical damage in ROS membranes and of possibly restoring the functional integrity of the ROS membranes.

MATERIALS AND METHODS

Purification of Plasma and Disk Membranes from Retinal ROS Cells. Purified rhodopsin-rich disk and plasma membranes from bovine ROS tissue were prepared following a modification (Smith et al., 1991) of the method of Molday and Molday (1987). Bovine eyes were transported frozen in ice, and retinas were removed and processed within 3 h postmortem. Postmortem effects are very minimal or negligible as evident from previous studies (Broekhuyse, 1968; Rothchild et al., 1980b; Feeney-Burns et al., 1984; Hicks & Molday, 1985). Briefly, ROS cells were treated with neuramindase to expose ricin-binding sites. Ricin–agarose was used instead of ricin–gold–dextran as suggested by Boesze-Battaglia and Albert (1989) to bind to plasma membranes. The outer segments were hypotonically lysed. Trypsin proteolysis was employed to enhance the plasma membrane yield by facilitating the separation of the disks from the plasma membranes. The disk membranes were harvested as an upper layer orange band from the plasma membrane pellet bound to the ricin–agarose beads using sucrose density gradient centrifugation. The plasma pellet was resuspended in β-methylgalactose and eluted through a ricin–agarose column to dissociate it from ricin beads. The disk and plasma membranes thus obtained were washed twice with cold deionized water to remove sucrose or any other buffer contamination. The membrane pellets were stored in liquid nitrogen. The technique provides the means by which the ROS plasma membranes can be isolated in an extremely pure state for spectral and biochemical characterization. Two sets of independent experiments each utilizing 100 and 160 bovine retinas were performed to determine the reproducibility of the methodology and consistency of the biochemical assay. ROS membranes prepared from these experiments were highly reproducible, and the fingerprint infrared spectra of the ROS membranes are virtually identical to the spectra of the partially bleached bovine ROS membranes obtained by Rotchild et al. (1980a,b) (see Figure 1). Our preparations are either partially or substantially bleached. A more comprehensive study of the dark-adapted retinas will be published elsewhere.

Extraction of Disk and Plasma Lipids. Retinal lipids were extracted from the disk and plasma membrane pellets using a modified Folch extraction (Borchman et al., 1989). All reagents were bubbled with argon to remove oxygen. Briefly, the retinal membranes were agitated vigorously with a chloroform/methanol mixture (1:1, v/v) under argon atmosphere. The chloroform phase was evaporated, and the lipids were rectified in KCl/chloroform to remove lipophilic or membrane-bound proteins. This step was repeated twice to ensure complete removal of the membrane integral proteins. Purified disk or plasma lipids were checked spectroscopically for any protein contamination. The dried lipids were redissolved to a known concentration in chloroform and stored frozen in liquid nitrogen. The UV spectra of the retinal ROS phospholipids are very similar to those obtained by Shvedova et al. (1983). No sizable conjugated dienes, characterized by a peak around 232 nm, were evident, indicating retinal lipids in our preparations remained completely unoxidized. Since the yield from plasma lipids was very low, we present here a limited study of these membranes.

Sample Preparation and Instrumentation. Lipid bilayers were prepared by dispersing disk and plasma membrane lipids in aqueous or in D_2O buffer (5 mM HEPES containing 100 mM KCl, pH 7.4) as described earlier (Lamba et al., 1993a). Briefly, the lipid in chloroform was evaporated under argon and dispersed in HEPES buffer (approximately 150 mg/mL). Lipid samples were warmed to 70 °C for 1 h to ensure complete hydration. An aqueous drop of liposomes was layered on a 13-mm diameter AgCl infrared window and sandwiched by another window spaced by a 0.015-mm teflon spacer. The spacer enclosing the infrared windows maintains the humidity of the sample for several hours. The windows were loaded in a temperature-controlled cell mount (Anderson-Bolds, Cleveland, OH) for infrared study. Purified disk membrane samples were prepared in the same manner.

Retinal lipids were oxidized by *tert*-butyl hydroperoxide or TBH (100 μM/mg of lipid) as described earlier (Lamba et al., 1991a). Lipids were also oxidized by incubating retinal disk lipids (0.2 mg/mL) in aqueous saline buffer (100 mM NaCl) at pH 7.0, initiating the LPO reaction by adding Fe^{3+}/EDTA (166 μM) and freshly prepared ascorbic acid (333 μM). Control lipids received no Fe^{3+}/EDTA and ascorbic acid. More than 80% of the oxidation was complete within the first 30 min. To ensure complete oxidation, the reaction was terminated after 1 h by freezing the samples in liquid nitrogen. Frozen samples were then lyophilized, and the lipids were dissolved in methanol to measure conjugated polyenes, a marker of LPO products, using UV spectroscopy.

Infrared data were acquired with a Nicolet 7199C FTIR spectrometer equipped with a TGS detector. Approximately 200 interferograms were recorded, coadded, and apodized with a Happ-Genzel function prior to Fourier transform, yielding an effective resolution of 1.0 cm^{-1}. The buffer spectra were obtained essentially in the same conditions as those used to record lipid spectra. This gave us high-quality spectra and also permitted the recovery of extremely weak signals by digital

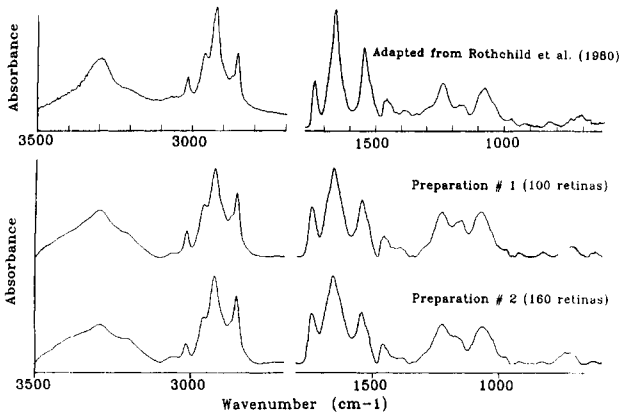

FIGURE 1: Fingerprint infrared spectra of bovine ROS membranes from two independent preparations utilizing 100 and 160 bovine retinas, respectively. The spectra obtained from thin films are virtually identical to the spectra of the partially bleached bovine ROS membranes obtained by Rothchild et al. (1980a,b).

subtraction of the buffer background (Lamba et al., 1993b). Temperature was controlled within ±0.1 °C by a copper-constantan thermocouple using a Fenewal variable temperature cell (Wilmad Glass, New Jersey). An average heating rate of 0.5 °C/min was maintained varying the temperature in steps of 5 °C with a waiting period of 15 min to avoid possible hysteresis of the phase transition. A nonlinear regression function described previously (Borchman et al., 1991) was used to fit the infrared lipid-phase transition curves. UV spectra were obtained with a 1-cm pathlength fused quartz cell on a Beckman DU-64 spectrophotometer.

Data Treatment and Analysis. All the necessary procedures of spectral routines performed in this work are essentially the same as those outlined in our recent publication (Lamba et al., 1993b). Signal averaging, data smoothing using the Savitsky–Golay procedure, base-line correction, buffer subtraction, difference and derivative spectroscopy, and related spectral routines were performed with the Spectra Calc. Software (version 2.22, Salem, NH). All the spectra presented in this paper are 11-point smoothed and were base-line corrected prior to buffer subtraction. Such numerical manipulations did not distort the line frequency, intensity, or shape of the bands.

RESULTS

Figure 1 shows the fingerprint infrared spectra of bovine ROS membranes from two independent preparations. The virtual similarity of the ROS membrane spectra shown in Figure 1 with those obtained by Rothchild et al. (1980a,b) suggests that ROS membranes not only are reproducible from preparation to preparation or from one laboratory to another but also demonstrate the consistency of the biochemical assay.

Figure 2 indicates the spectra of bovine ROS disk membranes (top) and disk lipids (middle) between 1800 and 1000 cm^{-1} dispersed in aqueous buffer, obtained after solvent subtraction. The solvent-subtracted infrared spectra of the disk membranes and disk lipids are very similar to the spectra of their anhydrous counterparts (spectra not shown). The solvent-subtracted spectra clearly indicate a multiple structure associated with sphingocarbonyls and the amide I band which otherwise remained obscured underneath the water band in aqueous solution. The bottom spectrum is generated by digital subtraction of the spectrum of the disk lipid from that of the disk membrane. The *positive peaks observed in the difference spectrum* in Figure 2 (bottom) are essentially those of pure rhodopsin and are characterized by strong amide I and II

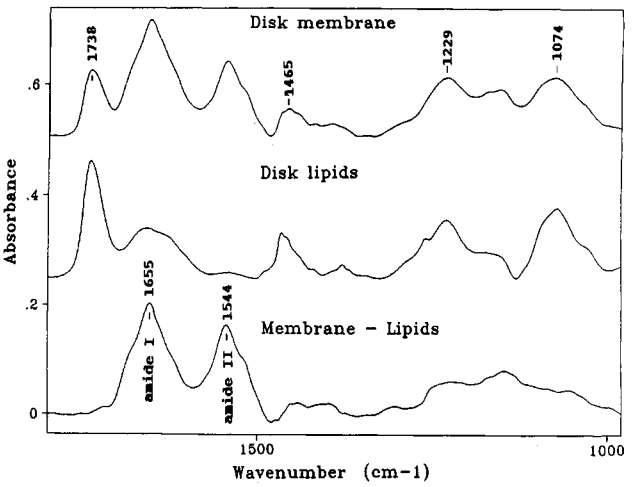

FIGURE 2: Fourier transform infrared spectra of bovine ROS disk membranes (top) and disk lipids (middle) between 1800 and 1000 cm^{-1} dispersed in aqueous buffer. Spectra are shown after solvent subtraction. The bottom spectrum is generated by digital subtraction of the spectrum of the disk lipid from that of the disk membrane.

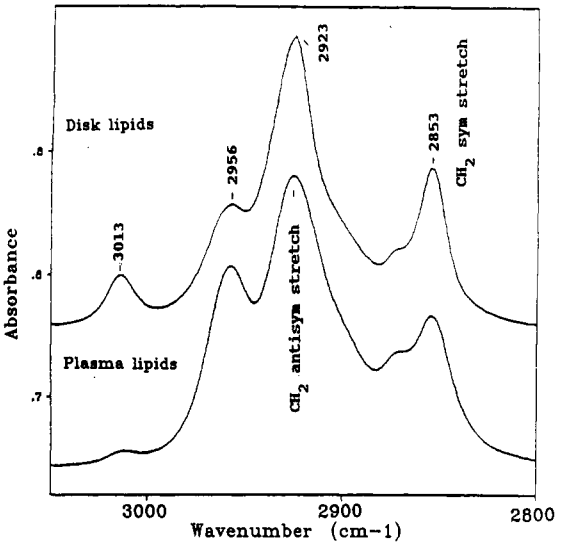

FIGURE 3: Fourier transform infrared spectra of the C–H region of bovine ROS disk and plasma lipids between 3100 and 2800 cm^{-1} dispersed in aqueous buffer after solvent subtraction. The 1736-cm^{-1} carbonyl peak solely due to phospholipids with a glycerol backbone is used for the purpose of normalization of the intensities. The positive peaks observed in the difference spectrum (bottom) are essentially those of a pure photoreceptor rhodopsin.

bands at 1655 and 1544 cm^{-1} (Rothchild et al., 1980b), respectively. These bands indicate the predominance of a helical conformation in rhodopsin situated in ROS membranes.

The carbonyl bands from both glycero- as well as sphingolipids absorb between 1800 and 1600 cm^{-1} in the infrared spectra of the interface region of the membrane bilayer, which serves as an interface between the hydrophobic lipid hydrocarbon chains and the hydrophilic lipid headgroups (Lamba et al., 1993a). Because of the differences in the interface linkage, the acyl-linked carbonyls of the lipids with the glycerol backbone exhibit a sharp asymmetric band around 1738 cm^{-1} and the amide-linked carbonyls with the sphingosine backbone absorb between 1670 and 1620 cm^{-1} (Lamba et al., 1993a). Using this characteristic carbonyl pattern, we have earlier distinguished two types of phospholipids in rabbit lens membranes (Lamba et al., 1993a).

Figure 3 indicates spectra of the C–H stretching region (3100–2800 cm^{-1}) of hydrocarbon chains of disk and plasma

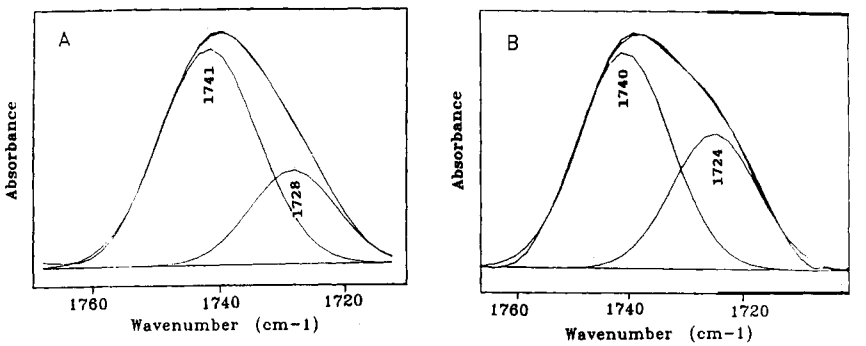

FIGURE 4: Resolution-enhanced glycerocarbonyl structure of bovine ROS in aqueous HEPES buffer in the 1800–1700-cm^{-1} region: (A) disk lipids and (B) disk membranes. Fourier self-deconvolution (FSD) was obtained assuming a Gaussian function of 10 cm^{-1} and a resolution-enhanced factor of 2.2. FSD data were curve fit assuming a Gaussian band profile of 15 cm^{-1}.

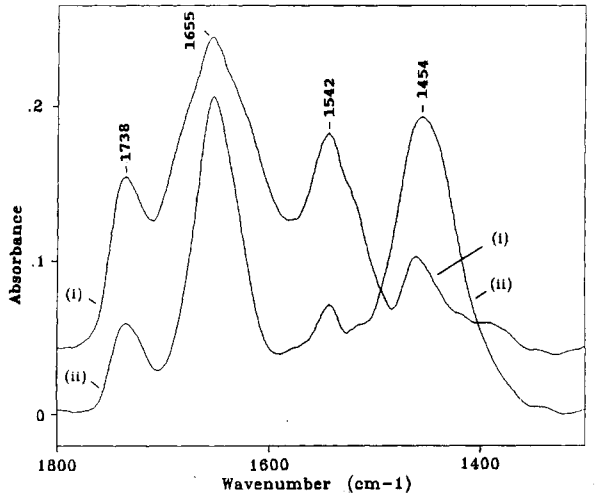

FIGURE 5: Fourier transform infrared spectra of the bovine ROS rhodopsin-rich disk membrane dispersions after solvent subtraction: (i) dispersed in HEPES aqueous buffer and (ii) dispersed in HEPES D_2O buffer.

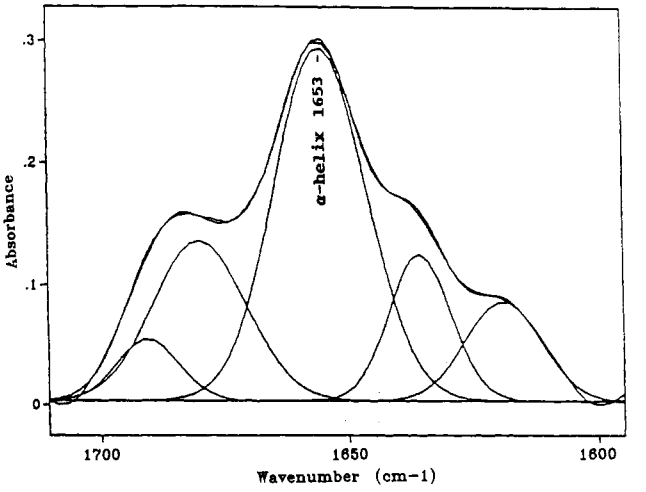

FIGURE 6: Fourier self-deconvolved/curve fit amide I band region (1710–1590 cm^{-1}) of the bovine photoreceptor rhodopsin. FSD was achieved assuming a Gaussian function of 10 cm^{-1} with a resolution-enhancement factor of 2.6. FSD data were then curve fit assuming a Gaussian band profile of 15 cm^{-1}.

lipids. A sharp band around 3013 cm^{-1} arises from the C—H stretch of the -HC=CH- moieties of the hydrocarbon chains (Rothchild et al., 1980b) in the spectrum of the lipids and is useful for assessing the degree of lipid unsaturation in membrane phospholipids (Lamba et al., 1993a). This band is also sensitive to perturbations arising from photobleaching, indicating the involvement of the hydrocarbon chains during rhodopsin photocascade (DeGrip et al., 1988). The other bands in this region are typical of the hydrocarbons of model phospholipids, and their origin and assignment are discussed in our earlier publications (Lamba et al., 1991a,b, 1993a).

Figure 4 shows the resolution-enhanced glycerocarbonyl region (1800–1700 cm^{-1}) of the ROS disk lipids (A) and disk membrane (B). The band profile clearly indicates asymmetry on the lower frequency side of the main band which is resolved into two components around 1740 and 1724 cm^{-1} upon curve fit. The extent of asymmetry in the C=O vibrations, their intensity ratio, and the magnitude of the carbonyl splitting provide a measure of the degree of the hydrogen bonding of the glycerocarbonyls (Hubner & Mantsch, 1991; Lamba et al., 1993a).

Figure 5 depicts the spectra, after solvent subtraction, of the rhodopsin-rich disk membranes dispersed in H_2O and D_2O buffers. In the spectrum of D_2O dispersions (curve ii), the amide II band shifts to 1454 cm^{-1}. The remnant amide II band intensity around 1542 cm^{-1} indicates the amount of unexchanged amino acid residues.

To quantitate the secondary structure of rhodopsin, we have Fourier self-deconvolved (FSD) and curve fit the amide I band profile of the rhodopsin as shown in Figure 6. Briefly, the amide I band was subjected to FSD to achieve the optimum number of components to be curve fit. A partial deconvolution of the amide I band was obtained with a series of resolution-enhancement factors k varying between 1.2 and 3.4. The optimal k value for the rhodopsin was chosen as 2.6 which yields FSD spectra free of sinusoidal lobes generated from overdeconvolution and/or higher resolution. These lobes, characteristics of the overdeconvolution, yield band components far exceeding the optimum number of components which could introduce a substantial error in structure analysis. This was avoided by carefully deconvolving the amide I band region as suggested by Surewicz and Mantsch (1988) and Susi and Byler (1988). The number of components and their approximate peak positions were also confirmed by obtaining a second derivative of the amide I band. The FSD spectra so obtained were curve fit assuming a Gaussian band profile of 15 cm^{-1} as shown in Figure 6. The error in the secondary structure analysis was no more than 6%.

Figure 7 depicts the phase-transition curve of the disk membrane which provides insight into the molecular mechanisms of the polymorphic phase behavior and dynamics of the hydrocarbon chains (lipid order and fluidity) in membrane bilayers. In Figure 8 are shown the phase-transition curves of the disk (A) and plasma (B) lipids. The solid curves are the controls, whereas phase curves with broken lines are those of the lipids oxidized with TBH (100 μM/mg of lipid).

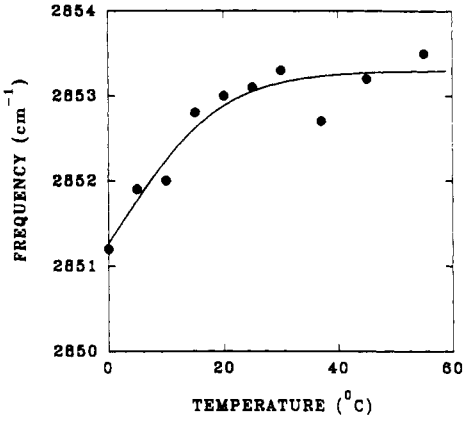

FIGURE 7: Infrared phase-transition curve of the bovine ROS disk membranes. The plot is constructed from the frequency measurement of the hydrocarbon CH_2-group modes around 2853 cm^{-1} as a function of temperature.

Figure 9 indicates the infrared spectra of the ROS disk lipids obtained after solvent subtraction. Top spectrum serves as a control. Lipids incubated with 100 μM TBH (bottom spectrum) indicate extensive damage to the membrane preparations.

DISCUSSION

Phospholipid Composition of the ROS Membranes. As indicated above, the spectrum of the disk lipids (Figure 2, middle spectrum) indicates a strong band around 1738 cm^{-1} characteristic of the glycerocarbonyls (Lamba et al., 1993a). Thus, disk membranes contain primarily glycerophospholipids such as: phosphatidylcholine (PC), phosphatidylethanolamine (PE), phosphatidylserine (PS), and phosphatidylinositol (PI) (Lamba et al., 1992). The sphingocarbonyl peak expected around 1660 cm^{-1} is very weak in the spectrum of the disk lipids (Figure 2, middle spectrum) and as such is merged within the bands expected from the cis conformation of the C=C double bond (Rothchild et al., 1980b) and the remnant bending mode of water molecules (Lamba et al., 1991b). This peak is also very weak in the spectra of the plasma lipids (spectra not shown) indicating a substantial lack of the sphingolipids both in the disk as well as in the plasma membranes. These findings are consistent with the biochemical assays of the phospholipid composition of the ROS (Fliesler & Anderson, 1983) and of the disk and plasma membranes (Boesze-Battaglia & Albert, 1992). Although distribution of phospholipids in the disk and plasma lipids is quite different, disk membranes are PE/PC dominated (about 42/45%) whereas plasma membranes are predominantly PC phospholipids, about 65% (Boesze-Battaglia & Albert, 1992).

Degree of Lipid Saturation in ROS Disk and Plasma Lipids. As suggested above, and shown in Figure 3, the relative intensity of the 3013-cm^{-1} band indicates that the hydrocarbon chains of the disk lipids are unsaturated by a *factor of 5* over the acyl chains of plasma lipids (Lamba et al., 1992). This is remarkably close to the value of 4.7 obtained from a biochemical lipid composition study of the bovine ROS lipids (Boesze-Battaglia & Albert, 1989). The higher degree of lipid saturation in the plasma membranes may be a factor of stronger lipid–lipid interactions than in the disk membranes. The difference in the phospholipid composition of the disk and plasma lipids is also manifested in their phase-transition studies given below.

Extent of Hydrogen Bonding and Carbonyl Environment. The glycerocarbonyl C=O stretch band is a doublet resolved at 1740 and 1724 cm^{-1} in the spectra of the disk lipids (Figure 4). Multiple carbonyl bands in the spectrum of disk lipids are indicative of the formation of structurally different molecular environments for the carbonyl groups. We calculate that about 23% of the carbonyls in the disk lipids participate in hydrogen bonding with bilayer water. These bound carbonyls are one-third higher in the disk membrane containing rhodopsin indicating that rhodopsin increases hydrogen bridges between lipid carbonyls and/or bilayer water molecules. The hydrogen-bonding network provides additional structural stability to the ROS membrane that pure lipid bilayers do not have.

Hydrocarbon Chain Structure and Acyl Chain Packing. The antisymmetric 2923- and symmetric 2853-cm^{-1} C–H stretch bands (Figure 3) suggest a significant difference in the lipid composition and structure of the disk and plasma membranes. These bands in the spectrum of plasma lipids are much broader than those of the disk lipids, which is characteristic of the lipid–lipid or lipid–cholesterol interactions. Thus, plasma lipids assume a more heterogeneous hydrocarbon chain structure than the disk lipids. Higher cholesterol (3-fold higher cholesterol/phospholipid ratio) and hydrocarbon saturation in the plasma membrane than those in the disk membrane (Boesze-Battaglia et al., 1989) would contribute substantially to a rigid phospholipid environment. Another significant difference in the hydrocarbon chain structure of the ROS lipids is the bands at the 2956- (antisymmetric) and 2872-cm^{-1} (symmetric) C–H stretches of the terminal methyl groups (Lamba et al., 1991b) which are more intense in the plasma lipids (Figure 3). This could be due to a large number of shorter hydrocarbon chain segments, and/or the acyl chains in these lipids could be exposed to the membrane bilayer, possibly due to higher cholesterol in the plasma membrane.

The relative amount of gauche rotamers at a given temperature is indicative of the level of disorder of a lipid bilayer (Cameron et al., 1980). This disorder of the membrane can be measured from the CH_2 frequency of the hydrocarbon chain. For a completely ordered system (all-trans CH_2 segments or 0% gauche rotamers), such as dispersion of dipalmitoylphosphatidylcholine at −20 °C, the CH_2 symmetric frequency is observed at 2849.0 cm^{-1}. The all-trans CH_2 order is completely destroyed when DPPC or any other lipid is dissolved in chloroform, and the corresponding CH_2 frequency is observed at 2854.5 cm^{-1}. The percentage of gauche rotamers thus can be estimated from the following equation:

$$\% \text{ gauche rotamers} = \frac{[(CH_2 \text{ sym stretch frequency}) - 2849.0] \times 100}{(2854.5 - 2849.0)}$$

From this equation, we estimate that both the plasma and disk membranes are significantly disordered (approximately 80% gauche rotamers) at physiological temperature. At this temperature, the all-trans fatty acyl carbon chains both in plasma and disk lipids are diminished mainly due to breakdown of van der Waals interactions, thereby increasing the number of C–C gauche rotamers. This disorder may facilitate the ability of rhodopsin to regenerate which not only depends on the position of the disk in ROS (Williams, 1985) but also upon the lipid environment (O'Brien et al., 1977; Morton et al., 1986).

A sharp band at 1468 cm^{-1} due to the scissoring mode of the CH_2 groups in the spectrum of the disk lipids (Figure 2, middle spectrum) indicates that the hydrocarbon chains of the lipids are packed in a hexagonal or triclinic unit cell in the ROS bilayers. This band is broader and appears at lower

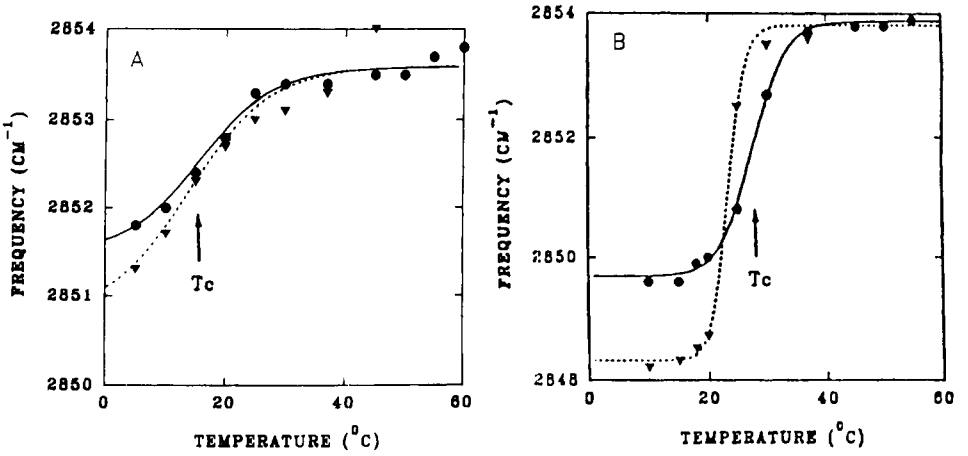

FIGURE 8: Infrared phase-transition curves of the bovine ROS lipids: (A) disk lipids and (B) plasma lipids; solid curves—control; broken curves—oxidized with 100 μM *tert*-butyl hydroperoxide (TBH). The plot is constructed from the frequency measurement of the hydrocarbon CH_2-group modes around 2853 cm^{-1} as a function of temperature.

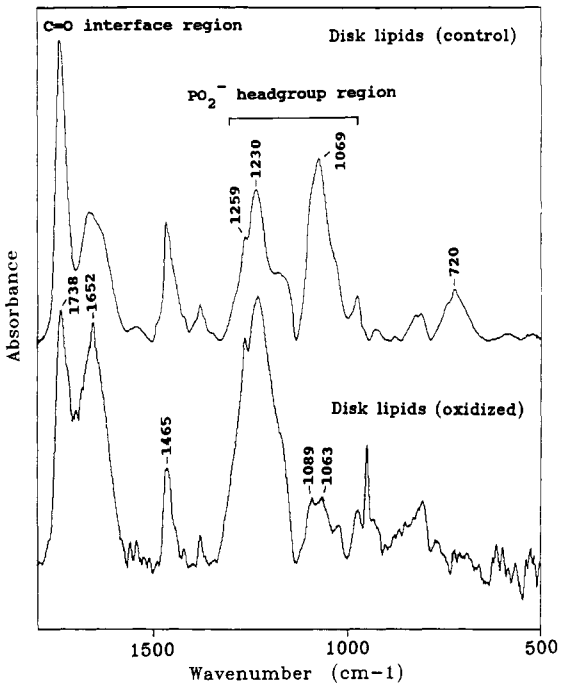

FIGURE 9: Infrared spectra of the ROS disk lipids after solvent subtraction: (i) control and (ii) incubated with 100 μM *tert*-butyl hydroperoxide.

frequency (3 cm^{-1}) in the spectrum of the disk membrane (Figure 2, top spectrum) compared to in the spectrum of the disk lipids. This indicates an increased interaction of the acyl chains with the rhodopsin.

Membrane Headgroup Region. The headgroup region being in contact with the aqueous environment provides a useful site to probe lipid–lipid and lipid–protein interactions in membranes. The spectrum of the disk lipids (Figure 2, middle spectrum) indicates two bands at 1225 and 1069 cm^{-1} due to the antisymmetric and symmetric stretches of PO_2^{-1} groups, respectively (Lamba et al., 1991b, 1993a). The phosphate bands shift toward higher frequency and get broader and diffused in the membranes containing rhodopsin (Figure 2, top spectrum) indicating that *rhodopsin does influence the lipid headgroup structure.* A shift of the phosphate modes to higher frequency concomitant with increased broadening is characteristic of the weakening of the hydrogen bonds (Lamba et al., 1991b) and the increased rotational disorder in the rhodopsin–lipid matrix. The phospholipid headgroups are 90% positively charged in the ROS membranes and are expected to make extensive contacts with negatively charged O–H groups of the water and/or contacts with rhodopsin amino acid side chains which may provide necessary structural stability to ROS membranes. The lipid hydrocarbon chains are directed toward the hydrophobic core of the rhodopsin located on seven helices spanning the membrane bilayer (Zorn & Futterman, 1971), and large hydrophobic interactions are expected which may play a dominant role in stabilizing the rhodopsin–lipid membrane–matrix.

Rhodopsin is rich in charged and polar amino acids especially at their aqueous-exposed cytoplasmic surface. The hydrophilic sequence connecting the transmembrane segments are uniformly positive, whereas the carboxyl terminal segments are near neutral. Local arrays of these surface charges probably provide the binding sites for interaction with cytoplasmic proteins. Incorporation of rhodopsin with numerous charged residues may change the effective membrane surface charge, but its effect on lipid structure is unclear.

Conformation of Photoreceptor Rhodopsin in ROS Membranes. The spectrum of the D_2O dispersion of the rhodopsin-rich disk membranes (Figure 5) indicates a residual amide II band intensity around 1542 cm^{-1} after an hour of deuterium exchange which reflects the amount of nonexchanging amide hydrogens in highly ordered structures of the membrane domains that are shielded from rapid H–D exchange. The Am II/Am I intensity ratio indicates that as much as 84% of the peptide residues in membrane-bound rhodopsin is accessible to D_2O solvent after an hour of exchange. These results are consistent with the 75% exchange of the partially bleached or light-adapted ROS membranes reported by Rothchild et al. (1980b). In dark-adapted retinas, a very low H–D exchange (about 23% at 26 °C after 1 h) is observed in ROS membranes, partly because a large number of hydrophobic residues is buried in the membrane interior (Osborne & Nabedryk-Viala, 1977). The hydrophobic interactions resulting from spatial orientation of the phospholipid hydrocarbon chains and hydrophobic residues would also retard the exchange rate. The H–D exchange in our light-adapted retinas is (3–4)-fold higher than those observed in dark-adapted retinas. It appears that photobleaching not only tranduces photons but opens up the "hydrophobic heart" of the rhodopsin which leads to solvent accessibility. Because of the fact that the secondary structure of rhodopsin does not change appreciably upon photobleaching (see below), the breakdown of hydrophobic interactions and/or tertiary and quaternary structures which stabilize rhodop-

sin–lipid matrix must facilitate the observed rapid H–D exchange in our samples.

As indicated above, the amide I (1655 cm^{-1}) and amide II (1542 cm^{-1}) bands in the spectrum of the disk membrane are exceptionally intense in the rhodopsin-rich disk membranes (Figure 5). On the basis of the band-narrowing procedures outlined above (see Results) and discussed earlier (Lamba et al., 1993b; Surewicz et al., 1993), the secondary structure of rhodopsin as analyzed in Figure 6 indicates an extensive α-helical (53%) peptide conformation, with little β-sheet (21%) and β-turns (18%). Rhodopsin exhibits a unique structure of seven membrane-spanning α-helices comprising about half of the molecular mass embedded in the lipid bilayer approximately perpendicular to the plane of the membrane. The high helical content observed in rhodopsin appears to be consistent with the topologically similar, transmembrane protein, purple membrane bacteriorhodopsin (halobacterium halobium) (Lee et al., 1987) and is similar to the values of the dark-adapted retinas predicted previously (Schichi & Shelton, 1974; Osborne & Nabedryk-Viala, 1977; Stubbs et al., 1976b).

No significant change in the helical conformation of the rhodopsin was observed between 5 and 60 °C (see Lipid–Membrane Phase Transition below). A slight rearrangement of the turns and β-sheet structure (less than 4%) occurs in going from the gel-to-liquid-crystalline-phase transition. Lack of major structural change indicates that rhodopsin assumes a very stable conformation in the lipid environment. This high thermal stability of the rhodopsin is not surprising as the conformation of this protein also remains unaltered when solubilized with nonionic detergents (Osborne & Nabedryk-Viala, 1978).

Lipid–Membrane Phase Transition. The ROS plasma and disk lipids undergo a broad phase transition around 26 and 16 °C, respectively (Figure 8, solid curves), which is indicative of the different phospholipid composition of the two membranes. The plasma lipids with high enthalpy melt at a higher temperature than the disk lipids, and this is consistent with the notion that a higher degree of hydrocarbon chain saturation shifts the transition toward higher temperatures. The data also indicate a more ordered and cooperative plasma lipid bilayer than the disk lipids in the gel phase. All these parameters are indicative of a rigid phospholipid environment and stronger lipid–lipid interactions (Borchman et al., 1991) for the plasma lipids. However, both disk and plasma lipids are considerably disordered and fluid around physiological temperature, consistent with the amount of gauche rotamer calculated above.

The high cholesterol in the plasma membrane could also account for the observed difference in the transition temperature. Cholesterol is generally considered to decrease the fluidity, but its effect on biological membranes is not unique. Besides cholesterol, several other factors such as headgroup and interface region composition, hydrocarbon chain saturation, and hydrocarbon length also determine the physical properties of a membrane. Cholesterol is known to broaden lipid-phase transition (Lippert et al., 1980). In completely saturated model membranes, cholesterol has also been shown to order lipids in the *fluid state* and disorder lipids in the *odered state* (Lippert et al., 1980). In a model which may closely resemble lens membranes containing unsaturated lipids, cholesterol is known to rigidify the membrane (Levin, 1984). Addition of cholesterol in bovine lens lipids decreases the phase transition, enthalpy, cooperativity, and structural fluidity, whereas it increases the lipid order in a structural sense (unpublished data; Borchman et al., 1993). A structural fluidity could be different from a dynamic fluidity of the membrane. The higher cholesterol content in the plasma lipids compared to in the disk lipids factors to order plasma membranes. Insertion of the cholesterol molecule in the ordered lipids decreases the lipid–lipid interaction through weakening of the van der Waals contacts between the lipids. Similarly, double bonds disrupt the van der Waals interactions between lipids and cause them to melt at lower temperature and disorder the membrane. Thus, *a higher degree of unsaturation* could be a factor in fluidizing disk membranes.

The lipid-phase transition of the disk membranes containing rhodopsin is difficult to assess because of the lack of gel-phase data below freezing temperature. We estimate that the transition temperature is somewhere in the vicinity of 0 °C, possibly below zero (Figure 7). This shift in transition temperature in going from disk lipids to disk membrane indicates a large drop in the enthalpy of the ROS membrane–matrix, presumably due to enhanced rhodopsin–lipid interactions. The lipids surrounding the rhodopsin are structurally disordered. This structural disordering of the membrane should not be confused with the probe studies that show rhodopsin immobilizes lipids, dynamically ordering them (Hong & Hubbell, 1972; Pontus & Delmelle, 1975; Brown et al., 1976; Stubbs et al., 1976a; DeGrip et al., 1979; Sklar et al., 1979). It is instances like this that compel investigators to define the term "fluidity" to avoid confusion. Occurrence of the low phase transition in vertebrate ROS membranes indicates that these membranes remain largely fluid over a wide temperature range, i.e., just from a few degrees above subzero temperatures. The high content of polyunsaturated fatty acids assures that the disk membranes are fluid, even around 0 °C. These results are fully consistent with the dynamic model of rhodopsin, i.e., rapid rotational and lateral diffusion of rhodopsin (Hong & Hubbell, 1972; Poo & Cone, 1973; Brown et al., 1976; Stubbs et al., 1976a; DeGrip et al., 1979; Sklar et al., 1979). The unique phospholipid environment, i.e., structurally disordered and dynamically fluid environment of the ROS membranes observed in the present study, may be essential for the photoreceptor function.

Oxidative Damage to ROS Membranes. We have noted earlier that oxidative damage to lens membranes may contribute to cataractogenesis, the only disease of the human lens (Lamba & Borchman, 1991; Lamba et al., 1991a; Borchman et al., 1992, 1993). The ROS membranes rich in polyunsaturated acids are more susceptible to oxidative damage than those of the lens membranes. The free-radical damage to ROS membranes was induced by: (i) TBH and (ii) Fe^{3+}/EDTA–ascorbate system. This damage characterized by a change in the thermodynamic parameters of the lipid-phase transition (Borchman et al., 1991) is assessed below.

(*i*) *Oxidation Induced by tert-Butyl Hydroperoxide.* TBH-induced changes are evident in the phase-transition plots of the oxidized disk and plasma lipids (Figure 8, broken curves). The computed phase-transition parameters indicate an increase in the magnitude and cooperativity of the transition and lipid order in the membrane gel phase. The transition temperature is, however, decreased by a few degrees in both the disk and plasma lipids, probably due to disruption of the van der Waals forces. The increased amount of oxidation caused extensive damage both to disk as well as to plasma lipids. This change in the lipid order could have a profound effect on ROS membrane fluidity and is capable of deranging the photoreceptor function.

TBH-induced structural changes can be seen in the infrared spectra of the oxidized disk lipids (Figure 9). The phosphate antisymmetric the 1225-cm^{-1} band has increased 2-fold, whereas the phosphate symmetric the 1069-cm^{-1} band has diminished 4-fold in intensity. Intensity loss of the 720-cm^{-1} band due to methylene rock and/or headgroup choline is also apparent in the TBH-treated disk lipids (Figure 9). The intensity change in the phosphate modes is indicative of a major structural rearrangement of the phosphate–choline moiety. These changes are consistent with the NMR data which have indicated a diminished signal or an intensity loss of the headgroup choline and associated protons in TBH-treated sphingomyelin vesicles (Lamba et al., 1991a). A sharp 3-fold increase in the 1652-cm^{-1} band possibly due to induction of free -C=C- double bonds and/or carbonyls is also evident in TBH-treated disk lipids (Figure 9). Increase in conjugated polyenes (i.e., formation of alternative double bonds) in UV and a marked change observed in the intensity of the carbonyl, -C=C- double bond, phosphate, and certain choline modes in the infrared are the characteristics of the accumulation of LPO products in ROS membranes. Accumulation of these products are cytotoxic in vivo and may impair ROS membrane photoreceptor function. These results are consistent with the changes expected from a free-radical attack at the designated sites viz. phosphate and carbonyl groups which are known to participate in the free-radical chain reaction in ocular tissues (Lamba et al., 1994). Similar results were observed in the rabbit cortical lipid vesicles with a headgroup composition similar to those of the disk lipids when oxidized by Fe^{2+}/Fe^{3+}–hydrogen peroxide system (Lamba et al., 1994). The fact that prominent lipid skeletal modes such as C–H stretch/bend, phosphate, and carbonyl modes have not disappeared and/or reduced significantly in the oxidized samples suggests that membrane topography, i.e., headgroup, interface, and hydrocarbon chains, is still largely intact.

(ii) Oxidation Induced by Fe^{3+}/EDTA–Ascorbate System. Preliminary absorbance data (infrared and UV) indicate extensive damage to retinal membranes when exposed to potent oxidants such as the Fe^{3+}/EDTA–ascorbate system. The infrared structural changes are similar to those observed in the lipids incubated with TBH. Membranes incubated in the presence of Fe^{3+}/EDTA–ascorbate indicate a major change in the 270-nm peak characteristic of trienes, possibly through rearrangement of the six double bonds in docosahexanoic acid, whereas little change is observed in the 230-nm peak due to conjugated dienes (data not shown). These data indicate a chemical modification of the lipid and proteins of the ROS membranes, and it could be toxic if accumulated in vivo. Similar conclusions were reached earlier from a photodamage study of the ROS membranes (Shvedova et al., 1983). A noticeable difference is observed between the retinal and lens lipids upon oxidation. The lens lipids formed conjugated dienes when oxidized whereas retinal lipids formed conjugated trienes, possibly due to the presence of multiple double bonds in retinal lipids (Babyzhayev, 1989).

As indicated above, ROS membranes subjected to oxidative stress inflict extensive damage in vitro. Similar damage to ROS membranes is known to occur in vivo. In order to retard and/or possibly prevent this damage, we have developed a conjugated diene assay to determine the drug efficacy of the antioxidants. Such experiments are vital in understanding the disease process involving free-radical damage and oxidation associated with the ROS photoreceptor membranes. From a series of biochemical assays employed for screening antioxidant activity of the drugs available commercially as well as those procured from Alcon Inc. (Fort Worth, TX), the oxidative loss of the polyunsaturated fatty acid depends upon the levels of antioxidant present in the system (Lamba, Borchman, and Garner, unpublished data). A low amount of α-tocopherol (1.0 μg/mg of lipid) completely restored the loss of the docosahexanoic acid (data not shown). Similar results were obtained with trolox, a vitamin E derivative, and butylated hydroxytoluene (BHT). Many of the Alcon drugs have indicated drug efficacies better than that of α-tocopherol. These findings suggest that α-tocophenol protects against lipid oxidation, possibly maintaining the functional integrity of the ROS membranes. The drug efficacy of the ROS membrane preparations with or without rhodopsin is in progress to assess the role rhodopsin might play in understanding the underlying diseases of the retinal disorders.

REFERENCES

Anderson, R. E.; & Maude, M. B. (1971) *Arch. Biochem. Biophys. 151*, 270–276.

Armstrong, D. (1984) in *Free Radicals in Molecular Biology, Aging and Disease* (Armstrong, D. et al., Eds.) pp 137–182, Ravin Press, New York.

Babizhayev, M. A. (1989) *Graefes* Arch. *Clin. Exp. Ophthalmol. 227*, 384–391.

Babizhayev, M. A., & Deyev, A. I. (1989) *Biochim. Biophys. Acta 1004*, 124–133.

Bazan, N. G., & Scott, B. L. (1987) in *Degenerative Retinal Disorders: Clinical and laboratory investigations*, pp 103–118, Alan R. Liss, Inc, New York.

Boesze-Battaglia, K., & Albert, A. D. (1989) *Exp. Eye Res. 49*, 699–701.

Boesze-Battaglia, K., & Albert, A. D. (1992) *Exp. Eye Res. 54*, 821–823.

Boesze-Battablia, K., Hennessey, T., & Albert, A. (1989) *J. Biol. Chem. 264*, 8151–8155.

Boesze-Battaglia, K., Albert, A. D., & Organisciak, D. (1992) *Invest. Ophthalmol. Visual Sci. 33*, (Suppl.), 1184.

Borchman, D., Delamere, N. A., McCauley, L. A., & Paterson, C. A. (1989) *Lens Eye Toxic. Res. 6*, 703–724.

Borchman, D., Yappert, M. C., & Herrel, P. (1991) *Invest. Ophthalmol. Visual Sci. 32*, 2404–2416.

Borchman, D., Lamba, Om P., Salmassi, S., Lou, M. F., & Yappert, M. C. (1992) *Lipids 27*, 261–265.

Borchman, D., Lamba, Om P., & Yappert, M. C. (1993) *Exp. Eye Res. 57*, 199–208.

Broekhuyse, R. M. (1968) *Biochim. Biophys. Acta 152*, 307–315.

Brown, M. F., Miljanich, G. P., Franklin, L. K., & Dratz, E. A. (1976) *FEBS Lett. 70*, 56–60.

Cameron, D. G., Casal, H. L., Gudgin, E. F., & Mantsch, H. H. (1980) *Biochim. Biophys. Acta 596*, 463–467.

Carter-Dawsen, L., Kuwabara, T., O'Brien, P. J., & Bieri, J. G. (1979) *Invest. Ophthalmol. Visual Sci. 18*, 437–446.

DeGrip, W. J., Drenthe, E. H. S., van Echteld, C. J. A., de Kruijff, B., & Verkleij, A. J. (1979) *Biochim. Biophys. Acta 558*, 330–337.

DeGrip, W. J., Gray, D., Gillespie, J., Bobvee, P. H. M., Van den Berg, E. M. M., Lugtenburg, J., & Rothchild, K. J. (1988) *Photochem. Photobiol. 48*, 497–504.

Delmelle, M., & Pontus, M. (1975) *Visual Res. 15*, 145–147.

Feeney-Burns, L., Hilderbrand, E. S., & Eldridge, S. (1984) *Invest. Ophthalmol. Visual Sci. 25*, 195–200.

Fliesler, S., & Anderson, R. E. (1983) *Prog. Lipid Res. 22*, 79–131.

Hargrave, P. A. (1982) in *Progress in Retinal Research I* (Osborne, N. O., & Chader, G. J., Eds.) pp 1–51, Pergamon Press, Oxford.

Hicks, D., & Molday, R. S. (1985) *Invest. Ophthalmol. Visual Sci. 26*, 1002–1013.

Hong, K., & Hubbell, W. L. (1972) *Proc. Natl. Acad. Sci. U.S.A. 69*, 2617–2621.
Kagan, V. E., Shvedova, A. A., Novikov, K. N., & Kozlov, Y. P. (1973) *Biochim. Biophys. Acta 330*, 76–79.
Kamps, K. M. P., DeGrip, W. J., & Daeman, F. J. M. (1982) *Biochim. Biophys. Acta 687*, 296–302.
Lamba, Om P., & Borchman, D. (1991) Influence of Hydrogen Peroxide and Lipid Composition on Rabbit Lens Membrane Structure. Eye lens Membranes and Agings, in *Topics in Aging Research in Europe* (Vrensen, G.E.J.M., & Clauwaert, J., Eds.) Vol. 15, pp 113–122, EURAGE Press, Leiden.
Lamba, Om P., Lal, S., Yappert, M. C., Lou, M. F., & Borchman, D. (1991a) *Biochim. Biophys. Acta 1081*, 181–187.
Lamba, Om P., Borchman, D., Sinha, S. K., Lal, S., Yappert, M. C., & Lou, M. F. (1991b) *J. Mol. Struct. 248*, 1–24.
Lamba, Om P., Borchman, D., Garner, W. H., & O'Brien, Paul J. (1992) *Invest. Ophthal. Visual Sci. 33*, (Suppl.) 1008.
Lamba, Om P., Borchman, D., & Garner, W. H. (1993a) *Exp. Eye Res. 57*, 1–12.
Lamba, Om P., Borchman, D., Sinha, S. K., Shah, J., Renugopalakrishnan, V., & Yappert, M. C. (1993b) *Biochim. Biophys. Acta 1163*, 113–123.
Lamba, Om P., Borchman, D., & Garner, W. H. (1994) *Free Rad. Biol. Med.* (in press).
Lee, D. C., Herzyk, E., & Chapman, D. (1987) *Biochemistry 26*, 5775–5783.
Leibovitz, B. E., & Siegel, B. (1980) *J. Gerontol. 35*, 45–56.
Levin, I. W. (1984) Vibrational Spectroscopy of Membrane Assemblies, in *Advances in Infrared and Raman Spectroscopy* (Clark, R. J. H., & Hester, R. E., Eds.) pp 29–33, John Wiley & Sons, Chichester, U.K.
Lippert, J. L., Lindsay, R. M., & Schultz, R. (1980) *Biochim. Biophys. Acta 599*, 32–41.
Molday, R., & Molday, L. (1987) *J. Cell Biol. 105*, 2589–2601.
Morton, R. W., Straume, M., Miller, J. L., & Litman, B. J. (1986) *Biophys. J. 49*, 277a.
Noell, W. K. (1980) in *The Effects of Constant Light on Visual Processes* (Williams, T. O., & Baker, B. N., Eds.) pp 3–28, Plenum Press, New York.
Noordam, P. C., Killian, A., Oude Elferink, R. F. M., & deGier, W. J. (1982) *Chem. Phys. Lipids 31*, 191–204.
O'Brien, D. F., Costa, L. F., & Ott, R. A. (1977) *Biochemistry 16*, 1295–1303.
Organisciak, D. T., Hih-min, W., Zong-Yi, L., & Tso, M. O. M. (1985) *Invest. Ophthalmol. Visual Sci. 26*, 1580–1588.
Osborne, H. B., & Nabedryk-Viala (1977) *FEBS Lett. 84*, 217–220.
Osborne, H. B., & Nabedryk-Viala (1978) *Eur. J. Biochem. 89*, 81–88.
Ovchinnikov, Y. A. (1982) *FEBS Lett. 148*, 179–191.
Penn, J. S., & Anderson, R. E. (1987) *Exp. Eye Res. 44*, 767–778.
Pontus, M., & Delmelle, M. (1975) *Biochim. Biophys. Acta 401*, 221–230.
Poo, M. M., & Cone, R. A. (1973) *Exp. Eye Res. 17*, 503–510.
Rothchild, K. J., Sanches, R., Hsiao, T. L., & Clark, N. A. (1980a) *Biophys. J. 31*, 53–64.
Rothchild, K. J., DeGrip, W. J., & Sanches, R. (1980b) *Biochim. Biophys. Acta 596*, 338–351.
Rotstein, N. P., Ilincheta de boschero, M. G., Giusto, N. M., & Aveldano, M. I. (1987) *Lipids 22*, 253–260.
Schichi, H., & Shelton, E. (1974) *J. Supramol. Struct. 2*, 7–16.
Shvedova, A. A., Alekseeva, O. M., Kuliev, I. Y., Muranov, K. O., Kozlov, Y. P., & Kagan, V. E. (1983) *Curr. Eye Res. 2*, 683–689.
Sklar, L. A., Miljanich, G. P., Bursten, S. L., & Dratz, E. A. (1979) *J. Biol. Chem. 254*, 9583–9591.
Smith, S. B., St. Jules, R. S., & O'Brien, P. J. (1991) *Exp. Eye Res. 53*, 525–537.
Speth, V., & Wunderlich, F. (1973) *Biochim. Biophys. Acta 291*, 621–628.
Stubbs, G. W., Litman, B. J., & Barenholz, Y. (1976a) *Biochemistry 15*, 2766–2772.
Stubbs, G. W., Smith, H. G., Jr., & Litman, B. J. (1976b) *Biochim. Biophys. Acta 425*, 46–56.
Surewicz, W. K., & Mantsch, H. H. (1988) *Biochim. Biophys. Acta 952*, 115–130.
Surewicz, W. K., Mantsch, H. H., & Chapman, D. (1993) *Biochemistry 32*, 389–394.
Susi, H., & Byler, D. M. (1988) *Appl. Spectrosc. 42*, 819–826.
Wetzel, M. G., Fahlman, C., O'Brien, P. J., & Gustavo, D. A. (1990) *Exp. Eye Res. 50*, 89–97.
Wiegand, R. D., Joel, C. D., Rapp, L. M., Nielsen, J. C., Maude, M. B., & Anderson, R. E. (1986) *Invest. Ophthal. Visual Sci. 27*, 727–733.
Williams, T. P. (1985) *The Visual System*, pp 61–71, Alan R. Liss, Inc., New York.
Yeagle, P. L. (1989) *FASEB J. 3*, 1833–1842.
Young, R. W. (1988) *Surv. Ophthalmol. 32*, 252–269.
Zigler, J. S., & Hess, H. H. (1985) *Exp. Eye Res. 41*, 67–76.
Zorn, M., & Futterman, S. (1971) *J. Biol. Chem. 246*, 881–886.